CHAPTER

11

Reduced Single Neuron Models

OUTLINE

A principle that has proven fruitful in modeling neural systems is to consider the simplest model capable of predicting the experimental phenomenon under consideration. This approach allows one to capture the essential points of a particular phenomenon without obscuring the picture with unnecessary details. This is precisely the approach taken by Hodgkin and Huxley to model action potential propagation along the squid giant axon in terms of sodium and potassium conductances. We have also seen how a simplification of the Hodgkin–Huxley model to a two-variable reduced FitzHugh model allows to characterize the firing properties of the Hodgkin–Huxley system in terms of phase plane analysis (Exercise 4.6). A set of simplified models are often used as a first pass to study issues related to synaptic integration or the impact of subthreshold membrane conductances on the processing of sensory inputs by neurons. In this chapter, we first present the most elementary model usually employed to simulate neurons, called the leaky integrate and fire model. Next, we introduce a class of neurons that have the ability to fire short bursts of spikes and briefly discuss their role in information processing in the nervous system. Finally, we analyze two simplified models of bursting neurons that highlight different mechanisms of burst generation within a single neuron.

11.1 THE LEAKY INTEGRATE-AND-FIRE NEURON

The most widespread simplified model for the activity of single neurons in response to various inputs is the *leaky integrate and fire neuron* (LIF neuron). In this model, the conductances responsible for spike generation (g_{Na} and g_K in the Hodgkin–Huxley model) are ignored and the spiking mechanism is replaced by a potential threshold, v_{thres}. This means that the membrane potential follows the differential equation,

$$C\frac{dv}{dt} = -\frac{v}{R} + I, \quad t > 0, \tag{11.1}$$

where $I = I(t)$ is some stimulation current and we adopt the initial condition $v(0) = 0$. When $v(t_1) = v_{thres}$ reaches threshold a spike is emitted at t_1 and the potential is reset to zero. Note that at steady-state and without input current the membrane potential is equal to zero which corresponds to the resting membrane potential value of the model.

Subthreshold behavior. Below threshold, the membrane potential satisfies a linear differential equation that is none other than the passive patch equation of Chapters 2 and 3 (e.g., Eqs. (2.13) and (3.1)). Thus, the approximation made in the leaky integrate and fire model amounts to neglecting all active membrane conductances as well as the electrotonic structure of a neuron's dendritic tree. Furthermore, as in the example of §3.1 for sinusoidal stimuli the subthreshold membrane potential of the LIF neuron is a low-pass filtered version of its input.

Mathematics for Neuroscientists, Second Edition
DOI: 10.1016/B978-0-12-801895-8.00011-7

© 2017 Elsevier Inc. All rights reserved.

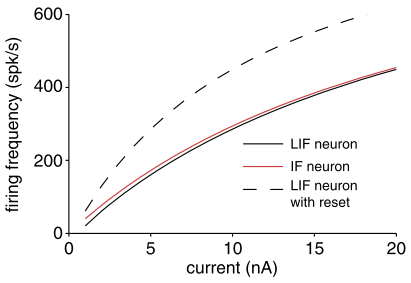

FIGURE 11.1 Firing frequency of a LIF neuron (black solid line; $R = 20$ MΩ, $\tau = 30$ ms, $t_{ref} = 1$ ms, $v_{thres} = 16$ mV), the corresponding IF neuron (red line) and a LIF with $v_{reset} = 8$ mV. (`fi_curves.m`)

f–I curve for constant current injection. We now compute the steady-state firing rate in response to a constant current pulse starting at $t = 0$. Eq. (11.1) implies an exponential relaxation to the steady-state value $v_\infty = IR$,

$$v(t) = IR(1 - \exp(-t/\tau))$$

with $\tau = RC$, the membrane time constant of Eq. (2.15). Thus, the injected current I has to be larger than the threshold current $I_{thres} = v_{thres}/R$ if the cell is to fire. For current above this value, the threshold potential is reached at that time, t_{thres}, for which $v_{thres} = IR(1 - \exp(-t_{thres}/\tau))$. That is, at

$$t_{thres} = -\tau \log(1 - v_{thres}/(IR)).$$

To mimic the refractory period observed in real neurons and in the Hodgkin–Huxley model, recalling Exercise 4.2, we enforce a period t_{ref} after the spike during which the membrane potential remains fixed at its reset value. If the model is endowed with such an absolute refractory period, t_{ref}, the firing rate is obtained from

$$f = \frac{1}{t_{ref} + t_{thres}} = \frac{1}{t_{ref} - \tau \log(1 - v_{thres}/(IR))}. \tag{11.2}$$

We infer from this formula that the firing rate saturates at a frequency $f_\infty = 1/t_{ref}$ in the limit of large injected currents (Figure 11.1).

Perfect integrator limit. In the limit of very high membrane resistance, we obtain a perfect integrator, or integrate and fire (IF) neuron, governed by the differential equation

$$C\frac{dv}{dt} = I(t).$$

In this case, past inputs are not forgotten over time and sum up perfectly. Under constant current injection the membrane potential grows at a rate I/C and thus reaches threshold when $v_{thres} = It_{thres}/C$ or equivalently the firing rate (without refractory period) is given by $f = I/Cv_{thres}$. When is the perfect integrator a reasonable approximation to the leaky integrate-and-fire neuron? This is only the case when the average time interval between inputs is small compared to the leaky integrate-and-fire membrane time constant τ, so that the output firing rate of the model is large compared to $1/\tau$. In this case, the capacitance does not have time to discharge significantly so that inputs do not get forgotten.

Synaptic inputs. Synaptic inputs to a LIF neuron can be simulated as simple instantaneous current inputs,

$$I_{syn}(t) = \sum_{n=1}^{n_{ex}} q_{ex}\delta(t - t_{ex,n}) + \sum_{n=1}^{n_{in}} q_{in}\delta(t - t_{in,n}). \tag{11.3}$$

This corresponds to n_{ex} excitatory inputs at times $t_{ex,n}$ and n_{in} inhibitory inputs at times $t_{in,n}$. Here q_{ex} and q_{in} represent the charge transferred instantaneously to the membrane capacitance by an excitatory or inhibitory input, respectively. On recalling Eq. (3.4) we note that each excitatory input spike increments the potential by q_{ex}/C. In

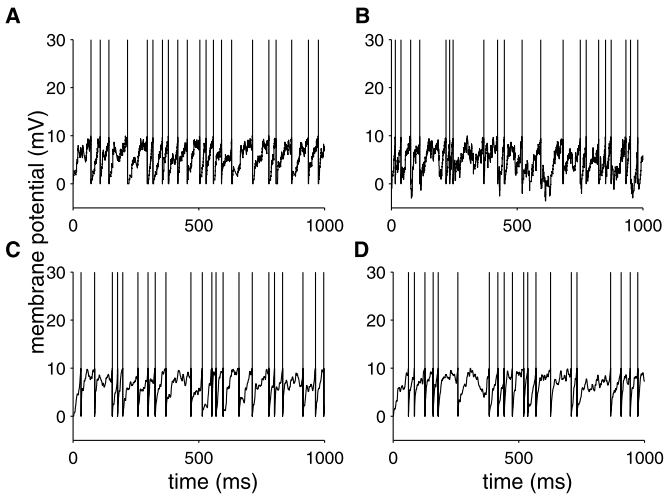

FIGURE 11.2 LIF membrane potential in response to random excitatory current-type synaptic inputs (**A**), a mixture of excitatory and inhibitory current-type synaptic inputs (**B**), excitatory conductance-type synaptic inputs (**C**) and a mixture of excitatory and inhibitory conductance-type inputs (**D**). See Exercises 1–4 for model parameters. Size of spikes is arbitrarily set 30 mV above rest. (`lif_rand_inp.m`)

order to compute the corresponding response we choose a time step, dt, and apply the Backward Euler Scheme to Eq. (11.1), with increments when an input spike has arrived in the last dt interval, and checks on refractoriness and threshold. More precisely, with $\vee_j \approx v((j-1)dt)$, we march according to

$$\begin{aligned} &\text{If not refractory then } \vee_j = \vee_{j-1}/(1+dt/\tau).\\ &\text{If fresh input has arrived then } \vee_j = \vee_j + (q/C)/(1+dt/\tau).\\ &\text{If } \vee_j \geq v_{thresh} \text{ then } \vee_j = v_{reset}. \end{aligned} \tag{11.4}$$

The reader will have an opportunity to code this in Exercises 1 and 2 and so reproduce panels A and B in Figure 11.2. Since synaptic input is more accurately modeled as a conductance change, we also consider stimuli of the form

$$I_{syn}(t) = \sum_{n=1}^{n_{ex}} g_{ex}(t, t_{ex,n})(v - v_{ex}) + \sum_{n=1}^{n_{in}} g_{in}(t, t_{in,n})(v - v_{in}), \tag{11.5}$$

where, e.g., each g is an α-function as in Eq. (2.18). Integration of this stimulus, in Exercises 3 and 4, will produce panels C and D in Figure 11.2.

Membrane potential reset after an action potential. The usual choice for the reset membrane potential v_{reset} after an action potential is the resting membrane potential, v_{rest}, which is equal to zero in Eq. (11.1). However, nothing forbids us from choosing a different reset value. If $v_{reset} \neq v_{rest}$, then the f–I curve of Eq. (11.2) depends on $\theta = v_{thres} - v_{reset}$ and its slope for high step currents is $\approx 1/C\theta$ (assuming $t_{ref} = 0$ and using $\log(1+x) \approx x$ for x small). Thus, the value of the reset potential allows one to control the slope of the f–I curve independently of v_{thres}. A second consequence of a high reset value is that the membrane potential hovers close to threshold and is thus much more sensitive to transient coincident inputs. This typically increases the variability of the spike train under random inputs.

Relative refractory period and threshold fatigue. Real neurons typically exhibit an absolute refractory period during which they will not fire and a relative refractory period during which the threshold for firing is elevated (Exercise 4.2 and Figure 17.3). A relative refractory period is sometimes implemented by incrementing the threshold after each

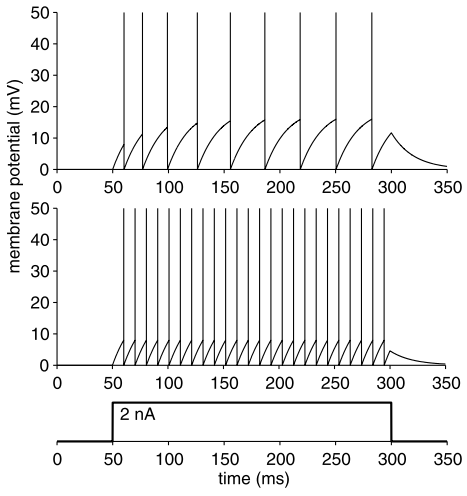

FIGURE 11.3 Response of a LIF with threshold fatigue (top) and without (middle) to a 2 nA current pulse (bottom; see Exercise 5 for model parameters). Spike height has been arbitrarily set to 50 mV above rest. (`thresh_fatigue.m`)

action potential and letting it decay towards its steady state value. More precisely,

$$\begin{aligned} &\text{If spiked} \\ &\qquad v_{thres} = v_{thres} + \delta v_{thres} \\ &\text{else} \\ &\qquad \frac{dv_{thres}}{dt} = -\frac{v_{thres} - v_{thres0}}{\tau_{v_{thres}}} \\ &\text{end.} \end{aligned} \tag{11.6}$$

We will put this scheme to use in Exercise 5 and achieve Figure 11.3.

Additional subthreshold conductances. Another common practice is to add additional subthreshold conductances to the LIF neuron to study their effect on the firing characteristics of the model. For example instead of modeling a relative refractory period as explained above, one can introduce a conductance that hyperpolarizes the cell following an action potential (abbreviated AHP for after-hyperpolarization) with a dependence on a slow varying variable like the calcium concentration. We will encounter such a conductance in our model of CA3 hippocampal pyramidal neurons in the next section, as well as in Figure 14.8.

11.2 BURSTING NEURONS

An important property of many neurons is their ability to generate short bursts of spikes. This points to the existence of ionic conductances that are able to activate and deactivate periodically on a time scale much slower than the action potential duration and thus drive the firing of small "packets" or bursts of spikes.

Intrinsic properties lead to different bursting behaviors. The ionic conductances responsible for bursting have been investigated in different cell types. It is now clear that several distinct mechanisms are at play.

1. Bursting can be caused by the activation of low-threshold conductances that are usually inactivated or closed at rest, such as the calcium permeable *T conductance* (I_T). Hyperpolarization of the membrane potential removes the inactivation or opens the channels and allows a depolarizing current to turn on, leading to "rebound excitation". A prominent example of this bursting mechanism are relay neurons in the thalamus discussed in the next section. In addition, other low threshold conductances such as for example the I_h current of §5.5 can play a similar role (see Figures 5.6 and 11.9 below).

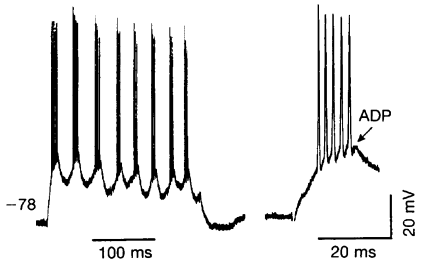

FIGURE 11.4 Intracellular recording from a chattering neuron in the visual cortex of the cat. In response to a depolarizing current pulse (0.9 nA) the cell generates a repetitive burst discharge of action potentials. The panel on the right is at an expanded time scale and shows an after-depolarization following the burst. Adapted from Gray and McCormick (1996).

2. A second widespread mechanism of bursting involves spatial interactions between the soma and dendritic compartments of a neuron. An example is given by CA3 pyramidal cells of the hippocampus that possess calcium channels localized in the dendritic compartments, but not the soma. A two compartment model of this bursting mechanism is analyzed in the next section. Upon current injection in the soma, the depolarization of the dendritic compartment is delayed in time with respect to the soma, causing significant current flow to and from the soma. Delayed activation of dendritic calcium conductances eventually sustains the depolarization of the soma causing the cell to burst (see Figures 11.10–11.12 below). A similar mechanism of bursting has been described in cortical neurons called *chattering cells* (Figure 11.4). In these neurons the burst frequency can be unusually high (up to 40 Hz) and relies on an interaction between soma and dendrites based on fast sodium conductances, instead of calcium conductances.
3. Dendritic morphology can play an important role in determining firing characteristics given a fixed set and distribution of conductances in various functional compartments of a neuron. An example that has been investigated in some detail includes various types of excitatory neurons of the cerebral cortex (pyramidal cells of different sizes, smooth and stellate cells). It has been shown by simulations that larger neurons with decoupled somatic and dendritic compartments are more prone to bursting than more compact neurons (Figure 11.5).
4. Although intrinsic properties can cause cells to burst, such effects are typically observed within networks of cells and the properties of bursts are thus in part determined by interactions among different neurons of a network (Figure 11.6).

Functional role of bursts. Bursts are thought to fulfill various functional roles in the nervous system. These include:

1. *Rhythm generation*. Many tasks such as for example locomotion, swimming or digestion of food involve the rhythmic activation of muscles. Such rhythms are typically generated by networks of neurons activated in definite sequences. Thus, both the intrinsic properties of nerve cells and their pattern of synaptic connections influence the generation of rhythms.
2. *Safety against unreliable synapses.* Bursts have long been thought to be effective at safely signaling important events. One reason is that synaptic transmission is stochastic and therefore often unreliable. Thus, stimulating repetitively a synaptic target offers a way to overcome this problem and assure that a message is delivered reliably. Therefore bursts of spikes could represent a "safety factor" in synaptic transmission. In cortex for example, layer 5 pyramidal cells are those most prone to burst and typically send long range connections toward other cortical or subcortical areas.
3. *Detection of sensory events.* Bursts could be used in sensory systems to signal important events; for example the occurrence of a salient object in the visual field (Figure 11.7).

11.3 SIMPLIFIED MODELS OF BURSTING NEURONS

We analyze two models in detail. The first one is a single compartment model of bursting in thalamic relay neurons that receive inputs from the sensory periphery and send their axons to cortical neurons. The second model is a two compartment model of pyramidal neurons of the hippocampus, a structure at the edge of the cerebral cortex that is thought to play an important role in learning and memory, as well as navigation.

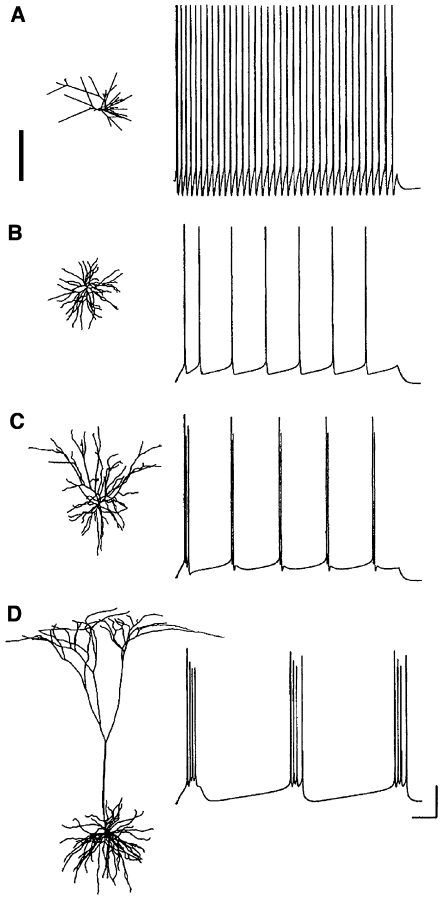

FIGURE 11.5 Model neurons with identical ion channel distributions generate distinct firing patterns according to their morphology. **A**. Layer 3 aspiny stellate cell of the rat somatosensory cortex. **B–D**. Layer 4 spiny stellate cell, layer 3 pyramidal cell and layer 5 pyramidal cell of the cat visual cortex, respectively. Scale bars: 250 μm, 100 ms, 25 mV. Adapted from Mainen and Sejnowski (1996).

Model of thalamic relay neuron bursting. Thalamic relay neurons have been extensively investigated as a model of bursting. We consider a single compartment model comprising several active conductances generating distinct currents: the fast sodium, I_{Na}, and delayed rectifier currents, I_K, that are responsible for action potentials, as well as a persistent sodium current, I_{NaP}, a low threshold calcium current, I_T, and a hyperpolarization activated mixed sodium/potassium current, I_h, like that encountered in §5.5. The differential equation governing the model is thus,

$$C_m \frac{dV}{dt} = -I_T - I_h - I_{Na} - I_K - I_{NaP} - I_L + I_{inj}, \tag{11.7}$$

where I_L is a leak (passive) current and I_{inj} represents the current injected through an electrode in the model.

The steady-state activation, s_∞, and inactivation, h_∞, variables for the low-threshold calcium current, I_T, are plotted in Figure 11.8 (Exercise 6). I_T is excitatory with a reversal potential $V_{Ca} = 120$ mV. Furthermore, I_T is essentially inactivated around the resting membrane potential of the model (≈ -65 mV), and thus does not influence the neuron's response to depolarizing inputs.

The steady-state activation, q_∞, and time constant, τ_q, functionals associated with I_h are plotted in Figure 5.6A. We recall, §5.5, that I_h is excitatory as well, since its reversal potential is above rest ($V_h = -40$ mV). However, it is only partially activated at rest. It also has the unusual property of further closing at depolarizing potentials and therefore plays a minor role in shaping the spike pattern of the neuron when it is depolarized from rest. Consequently, a constant, positive current pulse will mainly activate I_{Na} and I_K (and I_{NaP} to a lesser extent), causing regular spiking (Figure 11.9B; Exercise 7). In contrast a negative current pulse will activate I_h and relieve I_T from

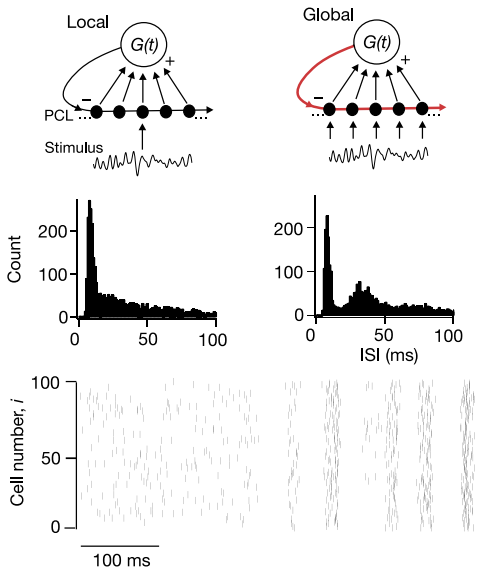

FIGURE 11.6 In the weakly electric fish *Apteronotus*, pyramidal neurons in the pyramidal cell layer (PCL) of a hindbrain structure called the electrosensory lateral line lobe encode information on random amplitude modulations of an external electric field (Stimulus). If a single cell is stimulated locally, it fires action potentials that are irregular, leading to an interspike interval distribution with a single peak (middle left). In contrast, simultaneous activation of many pyramidal cells through an extended (Global) stimulus, leads to two peaks in the interspike interval distribution resulting from bursting patterns of action potentials (middle right). This is caused by activation of strong inhibitory feedback (top left, red). Feedback activation by global stimuli also causes the pyramidal cells to synchronize or oscillate (bottom panels). These simulations summarize experimental results on the role of feedback described in Doiron et al. (2003).

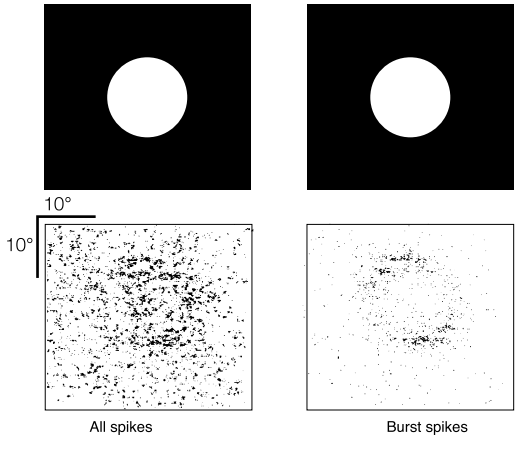

FIGURE 11.7 Burst spikes of visual cortical neurons recorded in monkeys reflect more clearly than all spikes what the animal was seeing. Bursts are defined as events consisting of two spikes less than 10 ms apart. The object was a static white disk on a black background (top). The screen of the video monitor covered 60 by 45 degrees of visual angle. The monkey was rewarded for following a fixation point, so that the receptive field of the cell could be positioned over the stimulus. Spikes were mapped in the lower panels according to the position of the recorded neuron's receptive field in space at their moment of occurrence. Adapted from Livingstone et al. (1996).

inactivation, causing a rebound depolarization leading to a burst of spikes well after termination of the current pulse (Figure 11.9A).

Note that since bursting can be described by a single compartment model it does not involve the more complex somato-dendritic interactions necessary to describe bursting in other cell types. In addition bursting in the model occurs on two different time scales: 7–14 Hz and 0.5–4 Hz, respectively, as observed in real neurons. These time scales correlate well with the kinetics of the T-type calcium current and the h-type mixed sodium/potassium current, respectively. Thus, the model suggests that activation of these currents is sufficient to explain the intrinsic bursting properties of thalamic relay neurons.

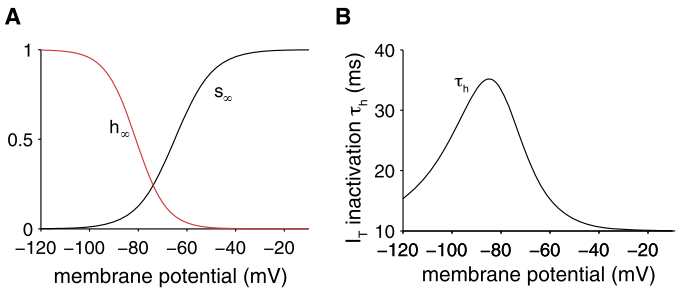

FIGURE 11.8 **A**. Steady-state activation, s_∞, and inactivation, h_∞, of I_T. **B**. Time constant of inactivation of I_T. (`wang_ss.m`)

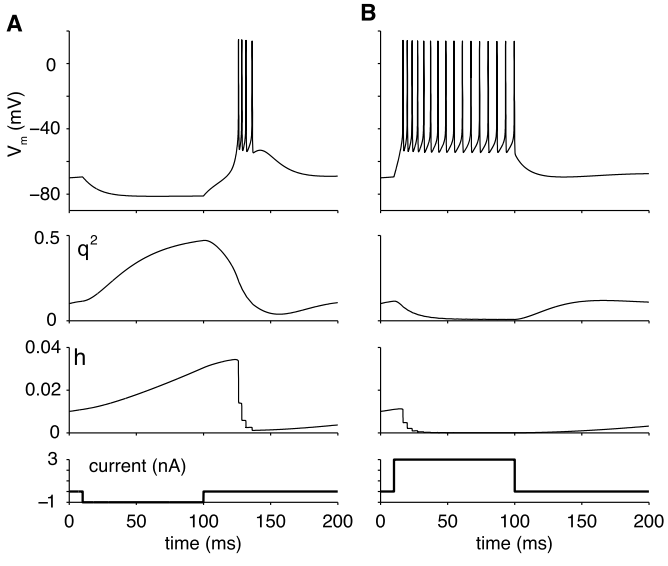

FIGURE 11.9 **A**. Response of the thalamic neuron model to a hyperpolarizing current pulse (-1 μA/cm^2, 90 ms long). From top to bottom: membrane potential, squared activation variable of I_h, inactivation variable of I_T and current pulse as a function of time. **B**. Response to a depolarizing current pulse ($+3$ μA/cm^2). (`wang_mod.m`)

Model of CA3 hippocampal pyramidal neuron bursting. This model is based on two compartments representing the soma and dendritic tree, respectively (Figure 11.10A). The somatic compartment corresponds to a fraction p of the total membrane surface area of the neuron and the dendritic compartment to $(1-p)$. To fit experimental data, the model requires $1/2$ of the surface area to be assigned to the somatic compartment. The somatic compartment is endowed with fast sodium and delayed rectifier conductances that can generate action potentials while the dendritic compartment has a voltage activated calcium conductance that can generate calcium spikes on a much slower time scale (Figure 11.10B). The differential equations for the membrane potential are as follows:

$$\begin{aligned} C_m V_s' &= -g_L(V_s - V_L) - I_{Na}(V_s) - I_K(V_s) + \frac{g_c(V_d - V_s) + I_s}{p} \\ C_m V_d' &= -g_L(V_d - V_L) - I_{Ca}(V_d) - I_{K,AHP}(V_d) - I_{K,C}(V_d) - \frac{I_{syn} - g_c(V_s - V_d) - I_d}{1-p}. \end{aligned} \tag{11.8}$$

All currents and conductances are expressed as densities, in units of μA/cm^2 and mS/cm^2, respectively. Thus, the coupling current between the two compartments that is proportional to $V_d - V_s$ and the injected somatic, I_s, and dendritic, I_d, currents, as well as the synaptic current, I_{syn}, are scaled by the fractional area of their respective compartments (p and $1-p$ for soma and dendrite, respectively). The parameters of the model are given in Exercise 8. In the dendritic compartment, both potassium currents, $I_{K,C}$ and $I_{K,AHP}$, depend on the intracellular calcium concentration of the dendritic compartment, $c = [Ca^{2+}]_d$. We suppose, for simplicity, that it is dimensionless. Its rate of change increases with $-I_{Ca}$ and decreases, e.g., through pumping mechanisms (see §14.2), that depend on c itself.

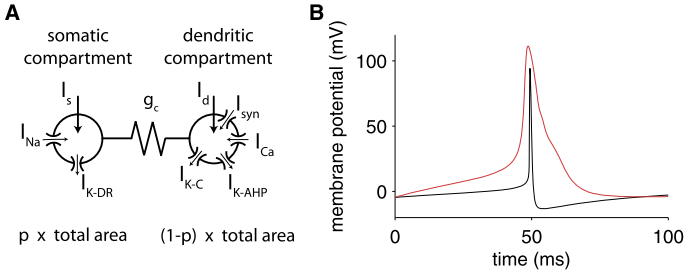

FIGURE 11.10 **A**. Schematic of the CA3 pyramidal cell model. Leak currents have been omitted for clarity. I_d and I_s represent currents injected through an electrode. **B**. Sodium (black) and calcium (red) spikes elicited in the isolated somatic and dendritic compartments ($g_c = 0$). The calcium spike was obtained by injecting a current of 0.68 µA/cm^2, while the somatic spike results spontaneously. (`pr_sodca_spike.m`)

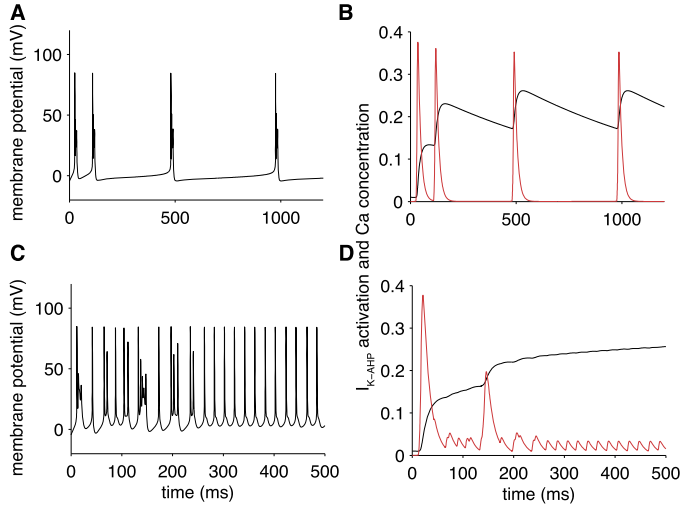

FIGURE 11.11 **A**. Somatic membrane potential in response to a somatic current injection (0.75 µA/cm^2). **B**. Time-course of the q variable governing activation of $I_{K,AHP}$ (in black) and calcium concentration (in red, arbitrary units, scaled down by a factor one thousand). **C**, **D**. Same as A, B but for a current injection of 2.5 µA/cm^2. (`pr_modes.m`)

To be precise, we suppose

$$c' = -0.13 I_{Ca} - 0.075 c. \tag{11.9}$$

The leading minus sign reflects the convention that inward currents are negative. In the absence of calcium current, c decreases exponentially towards zero with a time constant of $1/0.075 = 13$ ms.

The model possesses several distinct firing modes. For low somatic current injections, the model generates low frequency bursts (Figure 11.11A), whereas for higher currents the model generate regular spiking after an initial transient period (Figure 11.11C). In the first mode, a burst is triggered when the slow, hyperpolarizing current activation variable decreases below a threshold (Figure 11.11B), triggering a calcium spike in the dendrites. In the second mode, $I_{K,AHP}$ remains sufficiently high to prevent a dendritic spike (Figure 11.11D).

The dynamics of a burst is illustrated in Figure 11.12. It is initiated by a somatic spike because I_{Na} has a lower threshold than I_{Ca} (Figure 11.10B). This results in an initial current flow from the soma to the dendrite (Figure 11.12D, *i*) that activates I_{Ca}, below threshold for a calcium spike (Figure 11.12C, *ii*). As the soma repolarizes the current flow reverses from dendrite to soma (Figure 11.12D, *iii*), causing a second, smaller, somatic spike that stops the current drain from dendrite to soma (Figure 11.12D, *iv*) and allows a calcium spike to develop. The calcium spike triggers damped spikes in the soma as the sodium current is partially inactivated (Figure 11.12B, *v*) and the burst is finally terminated by the calcium dependent current $I_{K,C}$. After the burst, when the more powerful active conductances are turned off, the much smaller current $I_{K,AHP}$ controls again the dynamics of the inter-burst interval. Thus, in hippocampal CA3 pyramidal cells, bursting results from a complex interaction between active conductances in somatic and dendritic compartments.

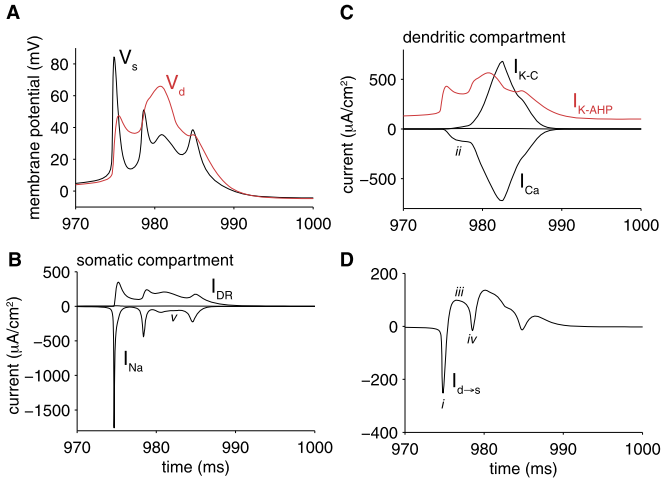

FIGURE 11.12 Detailed time-course of membrane potential and currents during a burst. Same simulation as in Figure 11.11A. **A**. Somatic and dendritic membrane potentials. **B**. Time-course of the somatic currents (leak current to small to see). **C**. Time-course of dendritic currents. $I_{K,AHP}$ has been scaled up by a factor 50. Leak current too small to see. **D**. Time-course of current from dendritic to somatic compartment. (`pr_complex.m`)

11.4 SUMMARY AND SOURCES

In this chapter, we have introduced several reduced single cell models. The leaky integrate and fire model goes back to Lapicque (1907). See Gerstner and Kistler (1992) for a thorough treatment. The leaky integrate and fire model is a basic workhorse used in countless theoretical studies of single neurons. See Fourcaud-Trocmé et al. (2003) and Brette and Gerstner (2005) for more recent non-linear generalizations. The two bursting models of §11.3 capture the essence of bursting based on two distinct biophysical mechanisms. The model of thalamic relay neurons is taken from Wang (1994) and that of CA3 pyramidal cells from Pinsky and Rinzel (1994). Both models are based on several decades of experimental and theoretical work. For extensive modeling of the hippocampus network, see Traub and Miles (1991). For a review of cellular and network mechanisms underlying thalamic activity see McCormick and Bal (1997). Bursting in thalamic relay neurons was originally studied by Jahnsen and Llinàs (1984). Weakly electric fish is one of the systems where the mechanisms, the information content and the behavioral implications of bursting have been best studied. See Turner et al. (1994) and Fernandez et al. (2005) for the biophysics of bursts in pyramidal cells and Laing et al. (2003) for a dynamical system perspective. For the implications of bursting on information coding and behavior, see Doiron et al. (2003), Oswald et al. (2004), Chacron and Bastian (2008) and Marsat et al. (2009). Krahe and Gabbiani (2004) reviews bursting across several sensory systems. We will return to simplified neuron models in §16.4 where we introduce a principled way of reducing the complexity of a high-dimensional compartmental model. The impact of random synaptic input on the membrane potential and firing rate of leaky integrate and fire neurons was briefly touched upon in Figure 11.2. We will study again the impact of random synaptic inputs on neuronal firing properties in Chapter 17 and with the help of reduced models in §19.4, once we have more powerful modeling tools at hand.

11.5 EXERCISES

1. Simulate a LIF neuron receiving random excitatory current-type synaptic inputs with parameters $\tau = 20$ ms, $R = 10$ MΩ, $v_{thres} = 10$ mV, $t_{ref} = 0$ and $v_{reset} = 0$. Simulate the model over 1 s, with a time step of 0.05 ms and assume that it receives $n_{ex} = 500$ excitatory inputs whose activation times are uniformly distributed over that interval, each with an associated charge $q_{ex} = 2$ pC. Use the marching scheme of Eq. (11.4) to reproduce Figure 11.2A.
2. Modify the model of the previous exercise to include current-type inhibition. Use the same model parameters, but assume that $q_{in} = 4$ pC and that the number of excitatory and inhibitory inputs over the 1 s interval is $n_{ex} = 660$ and $n_{in} = 100$, respectively (Figure 11.2B).

3. Replace the current-type synapse of Exercise 1 by an α-synapse. Assume $\tau_\alpha = 1$ ms and a reversal potential $v_{ex} = 70$ mV above rest. Use a peak conductance $g_{max} = Kq_{ex}$, where K is such that the total charge transferred by the synapse equals q_{ex} when the potential is clamped at its resting value. Use $n_{ex} = 600$ (Figure 11.2C).
4. Add inhibitory α-synapses. Use the same factor K as in the previous exercise and $q_{in} = 4$ pC as in Exercise 2. Assume $v_{in} = 0$ mV, $n_{ex} = 690$ and $n_{in} = 100$ (Figure 11.2D).
5. Simulate the response of a LIF neuron with threshold fatigue to a 250 ms long, 2 nA current pulse. Assume $C = 2$ nF, $\tau = 20$ ms, $v_{thres0} = 8$ mV, $\delta v_{thres} = 4$ mV, $\tau_{v_{thres}} = 80$ ms (Figure 11.3, top). *Hint*: Use a simple forward Euler integration scheme with $dt = 0.1$ ms.
6. Plot the steady-state activation and inactivation variables for I_T, given by $s_\infty(V) = 1/(1 + \exp(-(V + 65)/7.8))$ and $h_\infty(V) = 1/(1 + \exp((V - \theta_h)/k_h))$, with $\theta_h = -81$ mV and $k_h = 6.25$ mV^{-1}. Plot the effective inactivation time constant, τ_h/ϕ_h, with $\tau_h(V) = h_\infty(V)\exp((V + 162.3)/17.8) + 20.0$, and $\phi_h = 2$.
7. Implement the model of Eq. (11.7) using a hybrid Euler scheme. Compute the response to 90 ms long -1 μA/cm^2 and $+3$ μA/cm^2 current pulses, respectively (Figure 11.9). In Eq. (11.7), $C_m = 1$ μF/cm^2 and all variables are normalized per unit area (e.g., in the case of I_{inj}, μA/cm^2).
   The T-type calcium current is described by $I_T = \overline{g}_T s_\infty^3(V)h(V - V_{Ca})$, where the activation s is assumed to be instantaneously at equilibrium. The inactivation h and the other activation and inactivation variables described below are governed by the differential equation

$$dX/dt = \phi_X(X_\infty - X)/\tau_X(V) \tag{11.10}$$

   with $X = h, q, n$. ϕ_X is a temperature scaling factor that determines the effective time constant, τ_X/ϕ_X, of X. Assume $\overline{g}_T = 0.3$ mS/cm^2, $V_{Ca} = 120$ mV and see Exercise 6 for other values.
   The H-current is described by $I_h = \overline{g}_h q^2(V - V_h)$ with $\overline{g}_h = 0.04$ mS/cm^2 and $V_h = -40$ mV. The steady-state activation and time constant functionals are specified in Eq. (5.33). We assume $\phi_h = 1$.
   The potassium current is given by $I_K = \overline{g}_K n^4(V - V_K)$, with

$$\alpha_n(V) = \frac{0.01(V + 45.7 - \sigma_K)}{1 - \exp(-0.1(V + 45.7 - \sigma_K))} \quad \text{and} \quad \beta_n(V) = 0.125\exp(-(V + 55.7 - \sigma_K)/80)$$

   with $\phi_n = 200/7$, $\overline{g}_K = 30$ mS/cm^2, $V_K = -80$ mV and $\sigma_K = 10$ mV.
   The sodium current is given by $I_{Na} = \overline{g}_{Na} m_\infty^3(V)(0.85 - n)(V - V_{Na})$. The activation is assumed to be instantaneous and is replaced by its steady-state value. The inactivation h has been replaced by $(0.85 - n)$ as per Exercise 4.6. The constituents of m_∞ are

$$\begin{aligned} \alpha_m(V) &= \frac{0.1(V + 29.7 - \sigma_{Na})}{1 - \exp(-0.1(V + 29.7 - \sigma_{Na}))} \\ \beta_m(V) &= 4\exp(-(V + 54.7 - \sigma_{Na})/18) \end{aligned} \tag{11.11}$$

   with $\overline{g}_{Na} = 42$ mS/cm^2, $V_{Na} = 55$ mV and $\sigma_{Na} = 3$ mV.
   The persistent sodium current is given by $I_{NaP} = \overline{g}_{NaP} m_\infty^3(V)V - V_{Na})$ with $\overline{g}_{NaP} = 9$ mS/cm^2 and $\sigma_{Na} = -5$ mV in Eq. (11.11).
   The leak current is given by $I_L = g_L(V - V_L)$ with $g_L = 0.1$ mS/cm^2.
8. Implement the CA3 model of Eq. (11.8) using the MATLAB function `ode23` based on a Runge–Kutta integration scheme. The various currents of the model are defined as follows:

$$I_{Na}(V_s) = \overline{g}_{Na} m_\infty^2(V_s)h(V_s - V_{Na}), \quad I_K(V_s) = \overline{g}_K n(V_s - V_K), \quad I_{Ca}(V_d) = \overline{g}_{Ca} s^2(V_d - V_{Ca}),$$

   and two calcium dependent potassium currents

$$I_{K,C}(V_d) = \overline{g}_{K,C}\chi(c)r(V_d - V_K) \quad \text{and} \quad I_{K,AHP}(V_d) = \overline{g}_{K,AHP} q(V_d - V_K).$$

   The activation and inactivation variables obey

$$w'(V) = (w_\infty(V) - w)/\tau_w(V), \quad w_\infty(V) = \alpha_w(V)/(\alpha_w(V) + \beta_w(V)), \quad \tau_w(V) = 1/(\alpha_w(V) + \beta_w(V)),$$

with $w = h, n, s, r$ and q, respectively. The functions α_w and β_w are

$$\alpha_m = \frac{0.32(13.1 - V_s)}{\exp((13.1 - V_s)/4) - 1} \quad \text{and} \quad \beta_m = \frac{0.28(V_s - 40.1)}{\exp((V_s - 40.1)/5) - 1}$$
$$\alpha_n = \frac{0.016(35.1 - V_s)}{\exp((35.1 - V_s)/5) - 1} \quad \text{and} \quad \beta_n = 0.25\exp(0.5 - 0.025V_s)$$
$$\alpha_h = 0.128\exp((17 - V_s)/18) \quad \text{and} \quad \beta_h = \frac{4}{1 + \exp((40 - V_s)/4)}$$
$$\alpha_s = \frac{1.6}{1 + \exp(-0.072(V_d - 65))} \quad \text{and} \quad \beta_s = \frac{0.02(V_d - 51.1)}{\exp((V_d - 51.1)/5) - 1}$$

and

$$\alpha_c = \begin{cases} \exp((V_d - 10)/11 - (V_d - 6.5)/27)/18.975 & \text{when} \quad V_d \leq 50 \\ 2\exp((6.5 - V_d)/27) & \text{otherwise} \end{cases}$$
$$\beta_c = \begin{cases} 2\exp((6.5 - V_d)/27) - \alpha_c & \text{when} \quad V_d \leq 50 \\ \beta_c = 0 & \text{otherwise} \end{cases}$$

with $\alpha_q = \min(0.00002c, 0.01)$, and $\beta_q = 0.001$ and maximal conductances (in mS/cm^2)

$$g_L = 0.1,\ \overline{g}_{Na} = 30,\ \overline{g}_K = 15,\ \overline{g}_{Ca} = 10,\ \overline{g}_{K,AHP} = 0.8,\ \overline{g}_{K,C} = 15$$

and reversal potentials (in mV),

$$V_{Na} = 120,\ V_{Ca} = 140,\ V_K = -15, \quad \text{and} \quad V_L = 0.$$

The coupling parameters are $p = 0.5$, and $g_c = 2.1$ mS/cm^2. The capacitance is $C_m = 3$ μF/cm^2 and $\chi(c) = \min(c/250, 1)$. The stable rest state of the model is at the state-variable values of $(V_s, V_d, h, n, s, r, q, c) = (-4.6, -4.5, 0.999, 0.001, 0.009, 0.007, 0.01, 0.2)$, with the membrane potentials V_s and V_d relative to -60 mV.
Use the model to reproduce Figures 11.10B, 11.11 and 11.12 using the parameters given in the figure legends.